Emulsion synthetic route of hierarchically porous zeolite-geopolymer composites for Sr2+ decontamination in fixed bed process

Alban Gossard, Lilas Henriet, Samuel Vannier, Thomas David, Yves Barré, Agnès Grandjean

Ceramics International 50 (2024) 19692–19701

Contents lists available at ScienceDirect

Ceramics International

journal homepage: www.elsevier.com/locate/ceramint

Emulsion synthetic route of hierarchically porous zeolite-geopolymer composites for Sr^{2+} decontamination in fixed bed process

Alban Gossard [a,*], Lilas Henriet [a], Samuel Vannier [a,b], Thomas David [b], Yves Barré [a], Agnès Grandjean [a]

[a] CEA, DES, ISEC, DMRC, Univ. Montpellier, Marcoule, France
[b] Univ. Grenoble Alpes, CEA, LITEN, DTNM, LCAE, F-38000, Grenoble, France

ARTICLE INFO

Handling Editor: Dr P. Vincenzini

Keywords:
LTA zeolite
Geopolymer
Emulsion
Multiscale porosity
Strontium decontamination
Porous materials

ABSTRACT

The decontamination of wastewater is an important issue for the nuclear industry. The removal of Sr^{2+}, one of the most problematic radioelements, requires hierarchical materials suitable for fixed-bed processes. This article describes a patented emulsion-templating route for the synthesis of Linde Type A (LTA) zeolite-geopolymer composites with a multiscale porosity. By dispersing zeolite particles in an emulsion oil-in-water containing precursors of geopolymer, LTA zeolite–geopolymer composites can be obtained after curing and eliminating the oil phase. The zeolite particles alter the macroporous structure of the materials (replicating the oil droplets) as well as the size of the mesopores of the geopolymer binder. Moreover, zeolite contents higher than 30 wt% induce a crumbling of the material structure. The presence of LTA zeolite particles increases the selectivity of the composites for Sr^{2+} in very saline media, while the porous network of the material ensures rapid adsorption. The optimal composite prepared here outperformed a commercial sorbent for the Sr^{2+} decontamination of a saline wastewater through a packed column.

1. Introduction

Strontium-90 is one of the most common and hazardous radionuclides in wastewater produced by the nuclear industry. It can also be released when nuclear accidents occur such as the Chernobyl and Fukushima Daiichi NPP accidents. In both cases, large amounts of nuclear wastewater, often having complex compositions with competitive cations, need to be treated efficiently to limit the amount of secondary waste that then has to be stored. For that purpose, fixed bed decontamination processes are particularly adapted [1,2], and materials with specific properties are required to obtain ideal breakthrough curves. The bed materials must have a hierarchical and interconnected porous structure to optimize the transport properties of the ions of interest (diffusion) while limiting pressure drops (hydrodynamic flow) [3,4]. A selective active site (for example, a selective ionic exchanger) is also required to improve the extraction thermodynamic [5,6] and selectively trap contaminants under flow to limit the amounts of materials involved, which will be then secondary radioactive waste, and/or reduce treatment durations.

This paper reports the development of efficient hierarchical composites designed for Sr^{2+} decontamination of wastewater containing competitive cations such as Ca^{2+} and Na^{+}, under flow (in fixed bed processes). The composite is based on LTA zeolite, which is highly selective for Sr^{2+} over other cations (notably Ca^{2+} and Na^{+}) [7–11]. However, LTA zeolite is typically synthesized as a powder and cannot easily be shaped into a material suitable for fixed bed processes. In this way, the key objective is to obtain bulk or granular hierarchically porous materials containing LTA zeolite particles. Different methods have been described to integrate powdery materials in hierarchically porous and monolithic structures, including granulation [12], impregnating the particles or growing them in a pre-synthesized macrostructure [5, 13–15], or incorporating the powder into an ink before 3D printing [16].

The emulsion-templating approach also allows the incorporation of powdery materials in a porous structure [17–20]. The powder is incorporated in oil-in-water (O/W) emulsions stabilized by particles and/or surfactants. Depending on the formulation, the particles can contribute to the stabilization of the emulsion, and be adsorbed directly at the oil-water interface or homogenously dispersed in the aqueous phase [21–23]. A robust material with an interconnected macroporous network (replicating the emulsion droplets) can be obtained by growing

* Corresponding author.
E-mail address: alban.gossard@cea.fr (A. Gossard).

https://doi.org/10.1016/j.ceramint.2024.03.090
Received 15 December 2023; Received in revised form 6 March 2024; Accepted 7 March 2024
Available online 8 March 2024

a solid skeleton in the aqueous phase and eliminating the internal organic phase. The particles are therefore incorporated in the walls of the material and/or cover the surface of the macropores.

It has been previously demonstrated that O/W emulsions can be stabilized using a combination of LTA zeolite particles and tetradecyltrimethylammonium bromide (TTAB) [21,24]. The focus of the present study was on the next stage of the synthesis process: the consolidation of the continuous phase to as obtain hierarchically porous materials containing LTA zeolite particles. For that purpose, a geopolymer was chosen as a sufficiently robust backbone to be grown in the aqueous phase of the emulsion. Geopolymers are amorphous aluminosilicate materials, notably used in construction [25], as nuclear waste matrices [26,27], and in conventional liquid depollution [28]. They are synthesized from aluminosilicate sources such as metakaolin [29,30], and serve well as supports for zeolite particles [31] and more generally for powdery materials [32]. Geopolymers are obtained from a liquid solution containing dissolved precursors, which becomes a gel and then a mechanically robust material after condensation. This type of sol-gel reaction can be applied to emulsions, which solidify into a monolithic material [33–35] whose oil content can then be removed by thermal treatment, Soxhlet extraction or by using supercritical CO_2 [34,36,37]. If properly formulated, geopolymers have the interconnected mesoporous network [38] required to increase the accessibility of the LTA zeolite particles dispersed in their structure, and thereby improve the decontamination performance of the material [6,39,40]. Moreover, as geopolymer and zeolites are both inorganic aluminosilicate materials which could be directly incorporated in nuclear waste matrices, such adsorbents show promise for an optimized handling of the secondary waste induced by the decontamination operation [40].

This paper describes a recently patented emulsion-based route to synthesize a range of hierarchically porous geopolymers incorporating LTA zeolite particles [41]. We demonstrate the preparation of the composite materials and their application for Sr^{2+} removal from very saline nuclear wastewater in a fixed bed column. The microstructure of the materials was characterized to investigate its dependence on the LTA zeolite concentration and the formulation was optimized in terms of microstructure and Sr^{2+} selectivity by measuring the Sr^{2+} sorption properties of the materials.

2. Materials and methods

2.1. Chemicals

The LTA zeolite particles were synthesized from SiO_2 powder (Aerosil® 380, Evonik Industries, ≥99.5 % purity), NaOH pellets (Sigma-Aldrich, ≥97.0 %) and $NaAlO_2$ (VWR, 50–56 % of calculated assay as Al_2O_3) as precursor materials. The geopolymer phase was synthesized using metakaolin (Metamax, from BASF) as an aluminosilicate source, a commercial potassium silicate activation solution Betol® K 5020 T (Wöllner), and potassium hydroxide (VWR). Emulsions were produced using tetradecyltrimethylammonium bromide (TTAB, Sigma-Aldrich, ≥99 %) as the surfactant and dodecane (Sigma-Aldrich, ≥99 %) as the oil. The $Sr(NO_3)_2$, $Ca(NO_3)_2$ and $NaNO_3$ used in the sorption experiments were purchased from Sigma-Aldrich.

2.2. Synthesis of hierarchically porous geopolymers containing LTA zeolite particles

The LTA zeolite particles were synthesized as described previously [21,24]. The geopolymer precursors were mixed to obtain a final geopolymer with a molar composition of $SiO_2/Al_2O_3/K_2O/H_2O$ = 3.3/1/1/16. The appropriate amount of TTAB was mixed with LTA zeolite particles in deionized water. The LTA zeolite content was calculated to vary from 0 to 50 wt% of the final composite. The suspensions were placed in an ultrasonic bath for 1 h to disperse the zeolite particles and for the TTAB to reach adsorption equilibrium on the particles' surface. In the same time, potassium hydroxide pellets were dissolved in the potassium silicate solution. Both solutions were then mixed under magnetic stirring and dodecane was added to the mixture with a content set to 50 %vol. The all solution was homogenized using an IKA Ultra Turrax T25 homogenizer with a single rotor (S25N-18G) at 10 000 rpm for 1 min to form an emulsion. Metakaolin was added immediately after emulsification and the mixture was homogenized once more at 10 000 rpm for 1 min. A stable emulsion oil-in-water containing the composite precursors was obtained and left to rest in a closed mould for 48 h for the geopolymer structure to solidify. The material was then extracted from the mould and washed using a Soxhlet extractor (acetone/THF 50/50 %vol) for 24 h to remove the dodecane. The material was finally dried at 60 °C for 24 h.

In this work, the geopolymer material without LTA zeolite particles is referred to as MG (for macroporous geopolymer), while the composites containing LTA zeolite particles are referred to as MGZx (for macroporous geopolymer-zeolite), with x the zeolite mass percentage.

2.3. Materials characterization

X-ray diffraction (XRD) spectra were recorded at room temperature with an X'Pert PRO−PANalytical device with a Cu Kα-1 radiation source (λ = 1.5406 Å). Thermogravimetric analysis (TGA) and differential scanning calorimetry (DSC) were performed under airflow up to 700 °C at a heating rate of 10 °C•min^{-1} on a Mettler Toledo TGA-DSC 1 device. The macropores of the materials were observed by scanning electron microscopy (SEM). Routine measurements were performed on a FEI Inspect S50 instrument to estimate the global features of the macroporous networks. Finer observations of the MGZ27 sample were made using a Zeiss Gemini2 device with HE-SE2 and BSD4 A detectors. Before observation, the MGZ27 sample was coated with a non-reactive epoxy resin and it surface was levelled using automatic grinding/polishing machine. The electron energies ranged from 1 kV to 10 kV. Nitrogen adsorption-desorption isotherms were measured at 77 K using a Quantachrome Instruments NOVAtouch LX3 analyser. Specific surface areas were determined using the Brunauer-Emmet-Teller (BET) method and mesopore size distributions were calculated using the Barret-Joyner-Halenda (BJH) method.

2.4. Sorption experiments

Samples for the sorption experiments were prepared by grinding the materials and sorting grains that were 300–500 μm in diameter, the range of grain size typically used in packed columns [39]. The sorption experiments were performed in a saline matrix containing 0.25 M $NaNO_3$ and 1.25 mmol L^{-1} $CaNO_3$ (i.e. 50 mg L^{-1} Ca^{2+}) in deionized water. This solution composition was chosen to be representative of industrial nuclear wastewater, i.e. a saline solution containing competitive cations. Its pH was measured at 6.9. Note that geopolymers are particularly sensitive to the dissolution in acidic media [42]. Consequently, adsorbents described in this study are specially adapted for neutral or basic wastewater. The concentration of Sr^{2+} (from $Sr(NO_3)_2$) was adjusted as appropriate. The Sr^{2+} concentrations in the solutions before and after sorption experiments were analyzed by inductively coupled plasma - optical emission spectrometry (ICP-OES, ThermoFisher Scientific iCAP 6000 Series).

- Batch experiments

In preliminary experiments, estimated maximum sorption capacities were evaluated by contacting 1 g L^{-1} of materials for 24 h with the above described saline solution containing 200 mg L^{-1} Sr^{2+}. The sorption capacity Q (mg•g^{-1}) was calculated using the following equation:

$$Q = (C_i - C_f)\frac{V}{m} \quad (1)$$

where C_i and C_f are respectively the initial and final concentrations of Sr^{2+} in solution, V is the volume of the solution and m is the mass of material.

Estimated distribution factors (K_d = Q/Cf, in mL•g^{-1}) were then determined by contacting 1 g L^{-1} of materials for 24 h with the saline solution containing 2 mg L^{-1} Sr^{2+}. Indeed, radioactive Sr^{2+} in real liquid waste are present at the trace level, and distribution factor values are relevant for low Sr^{2+} concentrations. Note here that these experiments are only indicative of the impact of the zeolite on the Q and K_d values. The effective Q and K_d values will be defined for high and very low [Sr^{2+}] respectively and obtained thanks to complete sorption isotherms (see below).

Following these preliminary experiments, the most interesting materials were identified and more advanced analyses were performed. In the kinetic sorption experiments, 1 g L^{-1} of materials was contacted for different time intervals (5 min–48 h) with the model saline solution containing 50 mg L^{-1} Sr^{2+}. Sorption isotherms were measured by contacting 1 g L^{-1} of materials for 24 h with saline solutions containing 0.1–200 mg L^{-1} Sr^{2+}. Isotherm experiments reveal how Q and K_d vary with the initial Sr^{2+} concentration of the solution and thus their "real" maximum values (compared to the estimated values obtained previously) at very high and very low Sr^{2+} concentrations. Langmuir and Freundlich models can be used to fit the isotherms [6,40]. These models are described by Eq. (2) and Eq. (3) respectively:

$$Q_e = Q_{max}\frac{LC_f}{1+LC_f} \quad (2)$$

With C_f the final Sr^{2+} concentration at equilibrium (mg.L^{-1}), Q_e (mg.g^{-1}) representing the amount of Sr^{2+} adsorbed at the equilibrium and Q_{max} (mg.g^{-1}) the maximum adsorption capacity. L is the Langmuir constant.

$$Q_e = KC_f^n \quad (3)$$

With C_f the final Sr^{2+} concentration at equilibrium (mg.L^{-1}), Q_e (mg.g^{-1}) representing the amount of Sr^{2+} adsorbed at the equilibrium. K is the Freundlich constant and n an exponent, both related to the adsorption properties.

- Breakthrough curves

The performances of the MG and MGZ27 materials and a commercial LTA zeolite sorbent (supplied from Somez) were compared in a lab-scale column process. The column had an inner diameter of 10 mm and a packed height of 50 mm. The weights of sorbent were chosen to equalize the bed volumes. Breakthrough curves were measured using the saline solution with around 95 mg L^{-1} Sr^{2+} (determined exactly) at a flow rate of 20 mL h^{-1}, equivalent to a Darcy velocity of 0.25 m h^{-1}.

3. Results

3.1. Microstructural properties: influence of the LTA zeolite particles

3.1.1. Preliminary experiments: determination of the most efficient emulsion formulation and composite compositions

The water content of the geopolymer formulation was optimized to ensure it was sufficiently liquid to generate the mechanical shearing required for emulsification. The TTAB concentration in the emulsion was optimized to stabilize the emulsion, i.e. no visual observation of oil supernatant after shearing. As LTA zeolite particles adsorb TTAB in aqueous solution [21], the TTAB concentration was therefore increased proportionally to the zeolite weight percentage to keep the amount of free TTAB (i.e. free to adsorb at the aqueous solution-dodecane interface and thereby stabilize the emulsion) constant. The optimal dodecane content for the synthesis of highly macroporous materials was found to be 50 vol%. (the materials produced with a higher dodecane volume fraction were too friable). The zeolite content was varied 0 to 50 wt% of the final materials.

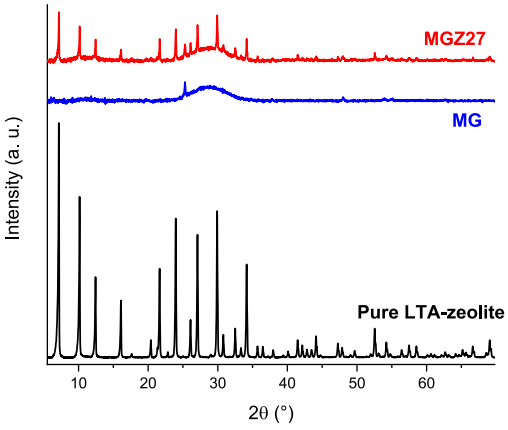

Fig. 1. X-ray diffractograms of the LTA zeolite particles (in black), and the MG and MGZ27 materials (in blue and red, containing 0 and 27 wt% LTA zeolite particles, respectively). (For interpretation of the references to colour in this figure legend, the reader is referred to the Web version of this article.)

TGA/DSC analyses confirmed the complete elimination of the oil phase and surfactant by Soxhlet washing (Figure S1 and S2). The X-ray diffractograms of the MG and MGZ27 materials are shown in Fig. 1 (for the sake of clarity, only those two are presented).

The broad hump between 24° and 34° for the MG material confirms that it is completely amorphous as expected, with the small crystalline peak due most likely to impurities initially present in the metakaolin [5]. For the MGZ27 composite material, the characteristic peaks of LTA zeolite superimposed on the broad hump confirm that the particles are well crystalline in the final material and adapted for selective ionic exchange with Sr^{2+} [10].

3.1.2. Microstructural effects of the LTA zeolite concentration

Fig. 2 shows the influence of the LTA zeolite particles content on the macroporous network of the materials.

The microstructure of the MG material (Fig. 2a) consists of an interconnected network of macropores of few tens of microns. These macropores are very well defined and replicate the emulsion droplets. The incorporation of zeolite particles in the material formulation induces a significant modification of the porous network. This is because the particles act as fillers [43] and are hydrophilic, they also absorb water in the precursor solutions. The geopolymer solutions with higher zeolite particle contents are therefore more viscous, hindering the shearing of the emulsion and increasing the geopolymerization speed [44]. The macropores are more irregular in shape, size, and spatial distribution, the more so the higher the zeolite content, with less rounded contours and a wider pore size distribution (Fig. 2b–d). Until around 27 wt% in zeolite (Fig. 2b and c), emulsion droplets replicas are still well identifiable. Nevertheless the pore size distribution enlarges with the zeolite content, with pores from few microns to several tens of microns. These latter come from poorly sheared droplets during the emulsification step. Then, for the highest zeolite contents (Fig. 2d), thin oil channels instead of perfectly round droplets replicas are observed, also in presence of very large pores, resulting in materials having inhomogeneous microstructures.

Higher magnification SEM images of the MGZ27 material (Fig. 3) shows the interconnectivity of the macroporous network, which appears in black in Fig. 3a. Moreover, as the geopolymer phase is mesoporous, the epoxy resin is able to penetrate in it (and not in the zeolite phase). Therefore, even if the geopolymer and LTA zeolites are both

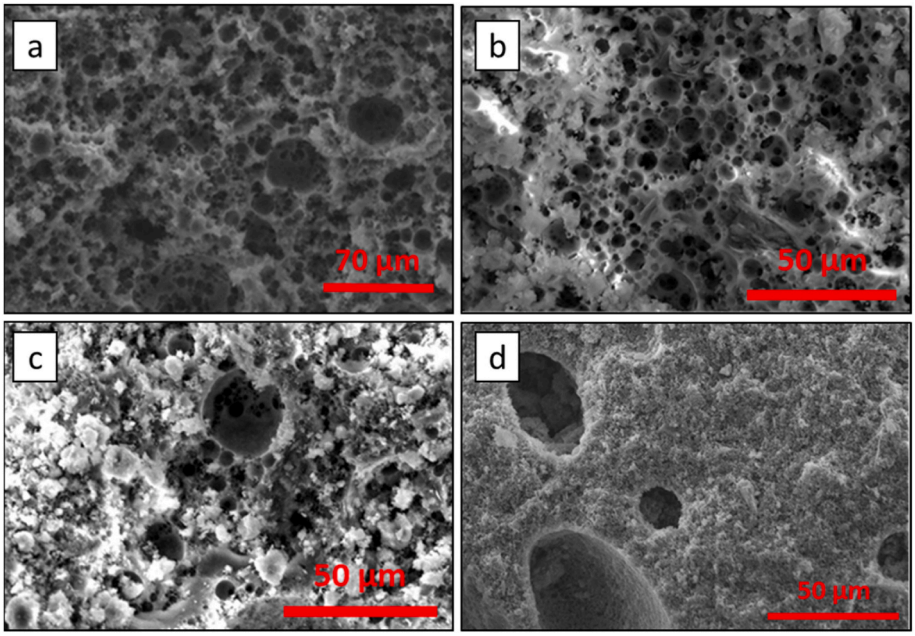

Fig. 2. Scanning electron micrographs of macroporous geopolymer materials containing (a) 0 wt%, (b) 14 wt%, (c) 27 wt% and (d) 38 wt% of LTA zeolite particles (MG, MGZ14, MGZ27 and MGZ38, respectively).

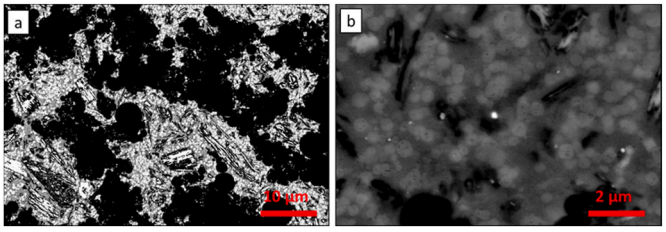

Fig. 3. Scanning electron micrographs of the macroporous geopolymer material with 27 wt% of LTA zeolite particles (MGZ27) at (a) low and (b) high magnification.

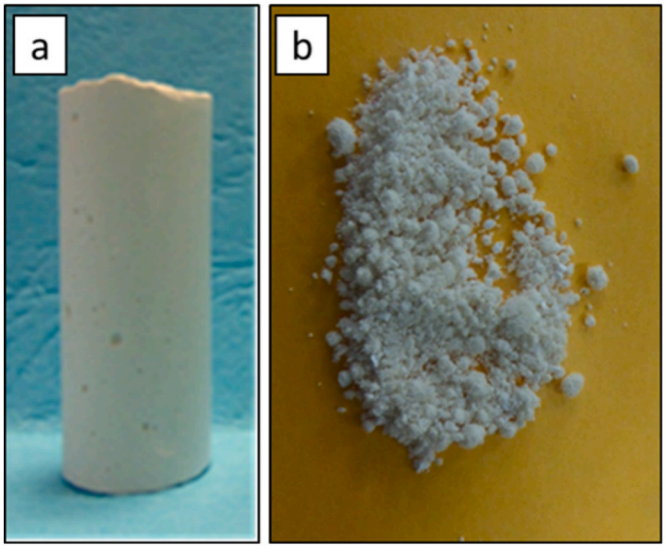

Fig. 4. Photographs of macroporous geopolymer materials with (a) 27 wt% and (b) 38 wt% of LTA zeolite particles.

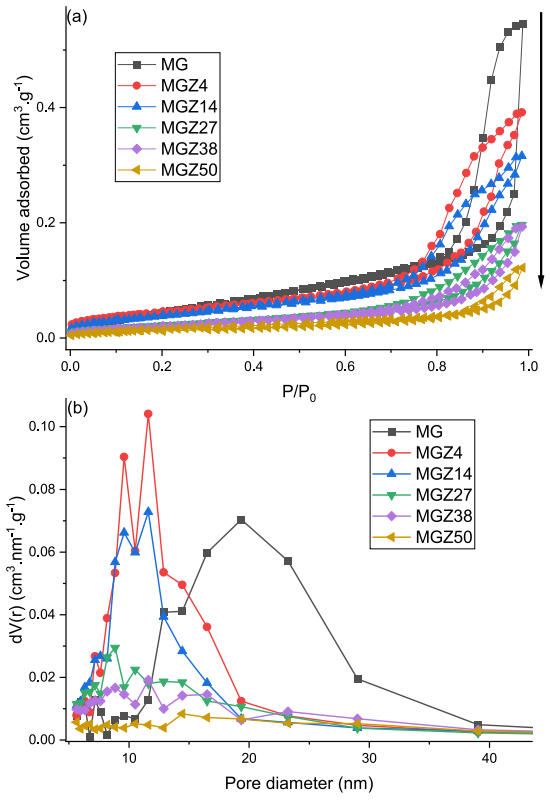

Fig. 5. (a) Nitrogen adsorption/desorption isotherms and (b) mesopore size distributions of macroporous geopolymer materials containing 0–50 wt% of LTA zeolite particles.

aluminosilicate materials, a difference of contrast is observed in Fig. 3b, highlighting the dispersion of the zeolite particles (white circular areas) in the geopolymer phase (brown binder). Note that these observations

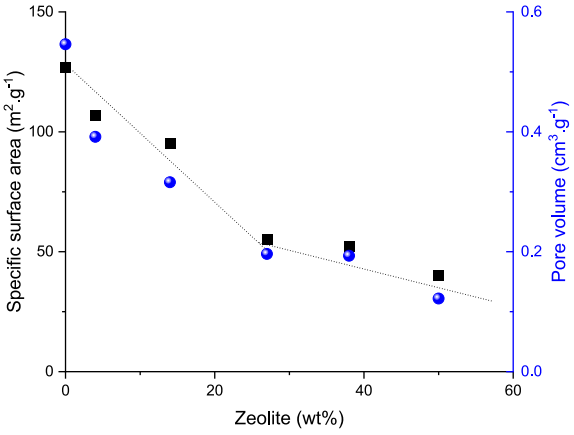

Fig. 6. Variation of the BET specific surface area (black squares, left y axis) and total pore volume (blue circle, right y axis) of the macroporous geopolymer materials as a function of their zeolite particles content. (For interpretation of the references to colour in this figure legend, the reader is referred to the Web version of this article.)

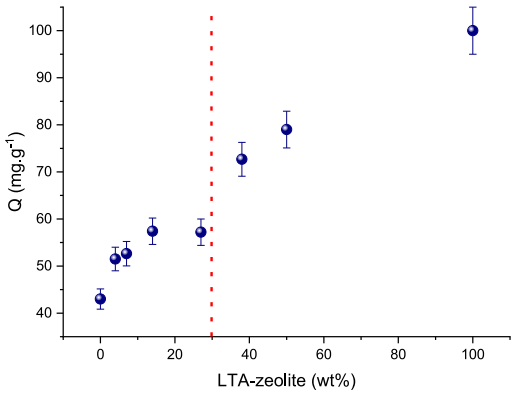

Fig. 7. Evolution of the extraction capacity of the MGx materials in a saline solution containing 200 mg L^{-1} of Sr^{2+} as a function of their zeolite content. The red dotted line represents the zeolite concentration above which the materials become friable. (For interpretation of the references to colour in this figure legend, the reader is referred to the Web version of this article.)

are consistent with the emulsion stabilization mechanism described previously for high TTAB concentrations [21,24]. Moreover, the shape of the zeolite particles are not destroyed by their loading in the geopolymer network compared to their initial shape described in literature [21,24]. This confirms that zeolite particles are not significantly degraded during the synthesis. Besides, the distribution of the LTA zeolite particles seems to be globally homogeneous in the geopolymer phase, although some aggregates are locally observed. It can be assumed that the presence of TTAB adsorbed on the zeolite particles surface may favor their dispersion in the continuous phase of the emulsion, and consequently in the final material.

Fig. 4 shows how a too large zeolite content affects the mechanical properties of the materials.

The robustness of the materials as a function of their zeolite content was visually evaluated. The materials containing low amounts of zeolite particles were monolithic and mechanically robust (Fig. 4a) while those with higher (more than 30 wt%) crumbled (Fig. 4b). Above a certain zeolite amount, indeed, the geopolymer content of the material is insufficient to properly bind the zeolite particles and support the monolithic structure.

Fig. 5 shows the nitrogen adsorption/desorption isotherms and mesopore size distributions obtained for the different materials.

The isotherms are all of type IV, which is typical of mesoporous materials [45]. Note that no micropores are observed because those in the Na-LTA zeolite are too small (0.41 nm) for nitrogen to enter [46]. The decrease in mesopore diameter associated with the presence of zeolite (Fig. 5b) may be explained by the hydrophilic nature of the zeolite particles, which are able to absorb water molecules from the geopolymer solution, reducing the amount available for geopolymerization and leading to smaller mesopores [47]. Fig. 6 presents the evolution of the total pore volume and BET specific surface area of the materials with the zeolite weight percentage.

Both total pore volume and specific surface area decrease with the amount of zeolite particles. The pore volume does not include micropores and the macropores, so their contributions can be assumed to be negligible. A first important drop of the pore volume is observed between 0 and 4 wt% of zeolites, due to both the smaller pore size induced by the water absorption by the zeolite, and the non mesoporous feature of the zeolite particles replacing and/or clogging parts of the mesoporous geopolymer walls. Then, until 27 wt% in zeolites, the decrease is more linear and proportional to the zeolite content, notably because the geopolymer mesopore size does not significantly evolve anymore. Finally, above 27 wt% zeolite particles, the more gradually decrease in pore volume can be explained by the release of some zeolite particles as the material crumbles (Fig. 4), thereby "re-opening" a part of the mesopores in the geopolymer. The evolution of the BET specific surface area with zeolite particles content presents only two linear evolutions, with no particular drop for the lowest zeolite amounts.

3.2. *Effects of the LTA zeolite concentration on Sr^{2+} extraction in batch mode*

Materials of this study present Sr^{2+} selective adsorption sites (LTA zeolite particles) and a multiscale porous network allowing the selective adsorption site accessibility in the wall of the geopolymer. These microstructural properties make these materials suitable for Sr^{2+} extraction in fixed bed processes and the best candidate was then identified by comparing their Sr^{2+} sorption properties in static batch experiments.

3.2.1. *Extraction performance at high and low Sr^{2+} concentrations*

The extraction capacity of the materials in a saline solution containing 200 mg L^{-1} of Sr^{2+} is plotted in Fig. 7 as a function of their zeolite content.

The geopolymer MG adsorbs Sr^{2+} ions even without zeolite particles, because the charge balancing cation (potassium) in the tetrahedral aluminosilicate network readily exchanges with other cations in aqueous solutions [48]. The Sr^{2+} sorption capacity increases roughly linearly with the zeolite content up to about 14 wt% and remains approximately constant until 27 %wt. Indeed, as mentioned above (Fig. 5), the porosity of the material is lower, which may reduce the accessibility for Sr^{2+} ion to a part of the sorption sites. Then, the sorption capacities of materials having more than 30 %wt of LTA zeolite particles increase again, which corresponds to the material crumbling. This leads to the collapse of the geopolymer-zeolite composites and more sorption sites become accessible again.

While both phases (geopolymer and LTA zeolites) contribute to the materials' sorption capacity, geopolymers are not selective for Sr^{2+} or other cations in saline media [49], such that two phases of the MGZx materials have to be considered separately when measuring the distribution coefficients (Kd): the geopolymer phase as a non-selective site and the LTA zeolite particles as selective sites. Assuming both phases are fully accessible to the Sr^{2+} ions, an expected $K_{d,calc}$ ($mL \bullet g^{-1}$) can be

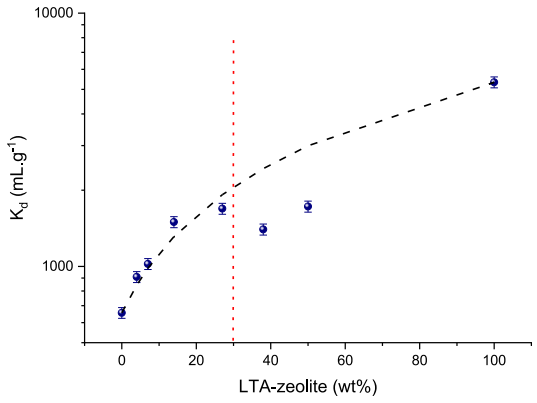

Fig. 8. Evolution of the distribution coefficients measured experimentally in a saline solution containing 2 mg L^{-1} Sr^{2+} (filled circles) and calculated using Eq. (4) (dashed line) as a function of the zeolite content of the materials. The red dotted line represents the zeolite concentration above which the materials become friable. (For interpretation of the references to colour in this figure legend, the reader is referred to the Web version of this article.)

calculated as a function of the zeolite content of the composites using the following Eq. (4):

$$K_{d,calc} = \%\frac{zeolite}{100} * K_{d,zeolite} + \left(1 - \%\frac{zeolite}{100}\right) * K_{d,geopolymer}. \quad (4)$$

Fig. 8 shows the evolution of the distribution coefficients measured for the materials in saline solutions containing 2 mg L^{-1} Sr alongside the values calculated using Eq. (4), as a function of the zeolite content of the materials.

The range of K_d values are lower than reported elsewhere in the literature [7,50–52], because the presence of high concentrations of competitive cations (Na^+ and Ca^{2+}) makes selective Sr^{2+} sorption more difficult. At zeolite concentrations up to 27 wt%, the experimental and calculated values overlap (Fig. 8). Thus, in term of selectivity, the composite material acts as two distinct phases for the Sr^{2+} extraction and the zeolite particles are well distributed and fully accessible in the mesoporous geopolymer network. Then, for zeolite concentrations higher than 27 wt%, the leveling-off of the capacity indicates that a part of the sorption sites of the geopolymer are less accessible due to the collapse of the porosity (Fig. 7). From this zeolite content, the K_d experimental values also deviate from the calculated line because some of the zeolite particles become inaccessible to the effluent and have no impact anymore on the selectivity. Nevertheless, contrary to the evolution of the capacity, the K_d values measured in the materials remain constant, when the materials start to crumble. Therefore, the sorption sites more accessible after material crumbing are geopolymer sites and not zeolite particles, which could remain agglomerate and stick together duo to their high concentration. However, these data are not representative of the composites themselves. Indeed, the distribution coefficients reflect the selectivity of the mixture, induced by the material collapse, of newly accessible pure geopolymer and remaining zeolite-geopolymer composites having inaccessible zeolite particles. These crumbled materials cannot be used in column processes and were therefore not investigated further. Monolithic materials with no crumbling was considered as sufficiently robust to be used in fixed-bed processes, while crumbled materials (with zeolite amount of more than 30 wt%) were not considered because of the risk of degradation during the decontamination operation and clogging of the column. Based on these results, the material offering the best compromise between mechanical robustness and extraction performance is MGZ27. The Sr^{2+} adsorption kinetic and thermodynamic of this material were therefore investigated more in detail in comparison with those of the geopolymer MG.

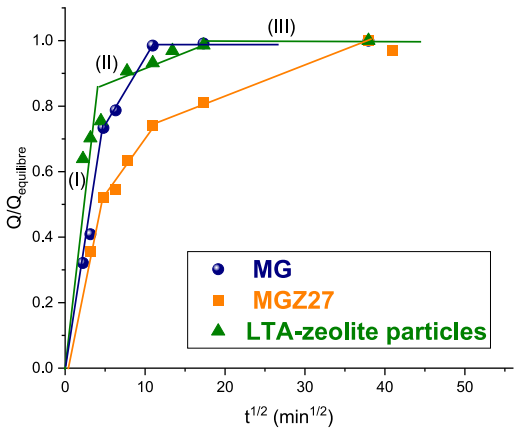

Fig. 9. Normalized adsorption capacities of the LTA zeolite particles (green triangles), the macroporous geopolymer (MG, blue circles) and the macroporous geopolymer material with 27 wt% of zeolite particles (MGZ27, orange squares) as a function of the square root of the contact time in a saline solution containing 50 mg L^{-1} Sr. (For interpretation of the references to colour in this figure legend, the reader is referred to the Web version of this article.)

3.2.2. Sr^{2+} adsorption kinetics of the zeolite particles as well as the MG and MGZ27 materials

The sorption kinetics of the MG and MGZ27 materials are compared with the LTA zeolite particles in Fig. 9. The capacities experimentally determined were normalized by the equilibrium capacity of each material and plotted as the square root of time to better illustrate the different mechanisms.

For the LTA zeolite particles, the equilibrium is obtained after 5 h and different steps are observed and described using the Weber and Morris model, which can be expressed using Eq. (5) and corresponds to successive diffusion limited steps highlighted by the linear evolution of the sorption capacity with the square root of time [40]:

$$Q(t) = k_{diff}.t^{1/2} + C \quad (5)$$

With Q(t) (mg.g^{-1}) the amount of Sr^{2+} adsorbed after a contact time t (min), k_{diff} the diffusion rate constant (mg.g^{-1}.$min^{-1/2}$), and C a constant linked to the thickness of the boundary layer.

The first step (I) corresponds to the diffusion in the liquid phase and through the boundary layer at the particles surface. As the particles are small, this step is fast. The second one (II) is related to the Sr^{2+} diffusion in the solid phase, i.e. in the microporous network of the zeolite particles, and is then consequently slower. Finally, an equilibrium step (III) is reached.

For the granular materials, the sorption kinetic is also divided in different steps. Nevertheless, due to their larger size (than the zeolite particles) and their porous structure, these steps can be attributed to different mechanisms than the zeolite powder. The first step of the kinetic consists in both the fast diffusion from the liquid phase to the surface and into the macro and mesoporous network, and through the boundary layer of both the external surface of the particles and the pores internal surface. Thus, the MG material having larger mesopores and porous volume than MGZ27 presents a faster kinetic during this first adsorption step. The second sorption mechanism corresponds to the diffusion of the contaminant in the solid phase of the adsorbents. Then, a transient step until the equilibrium is observed, which may be due to different sorption sites in the geopolymer phase. Indeed, due to their large grain size and the complexity of the geopolymer structure, this transient step could come from a slow diffusion through the whole

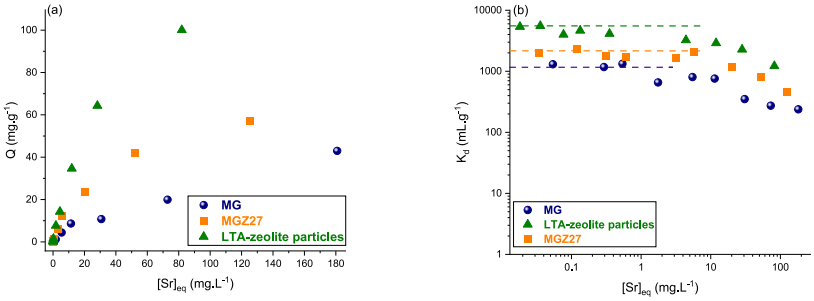

Fig. 10. Sr^{2+} adsorption isotherms: a) capacity and b) distribution coefficient as a function of equilibrium Sr^{2+} concentration, of the LTA zeolite particles (green triangles), the macroporous geopolymer (MG, blue circles) and the macroporous geopolymer material with 27 wt% of zeolite particles (MGZ27, orange squares), measured in saline solutions with different Sr^{2+} concentrations. The dashed lines are guides for the eye. (For interpretation of the references to colour in this figure legend, the reader is referred to the Web version of this article.)

material structure as the geopolymer walls are much larger than the zeolite particles (Fig. 3). Because they are controlled by the diffusion through the geopolymer walls, these two successive phases are relatively similar between MG and MGZ27. Finally, the equilibrium is quickly reached for MG and after 24–48 h for MGZ27, even if more than 80 % of the material capacity can be filled after 5 h.

3.2.3. Sr^{2+} adsorption isotherms on MG and MGZ27

Sr^{2+} adsorption isotherms were performed on the MG and MGZ27 materials as well as on the LTA zeolite particles. These isotherms can be presented as the evolution of the capacity as a function of equilibrium Sr^{2+} concentration (Fig. 10a) and fitted using a Langmuir or a Freundlich model [6,40] (see Figure S3). The Freundlich model fits the isotherm of the MG material, while the Langmuir model is better adapted for the LTA zeolite and the MGZ27. In accordance with the models, pure geopolymer may present different sorption sites and have complex sorption mechanisms [53] and the sorption of Sr^{2+} corresponds to an ionic exchange with Na^{+} in the crystalline cages of the LTA zeolite [8,11]. XRD analyses were performed on the materials after the Sr^{2+} adsorption step (Figure S4). No new crystalline phase was observed, supporting that Sr^{2+} is mainly adsorbed by ionic exchange, with a possible slight surface adsorption on the geopolymer phase [53]. As the sorption behavior of the MGZ27 follows the Langmuir model, the presence of zeolite particles seems to control the sorption mechanism of the composite. Thus, the Sr^{2+} adsorption at equilibrium is strongly impacted by the presence of the zeolite phase, even if both phases are involved.

However, for a nuclear decontamination application, the interest is more focused on wastewater containing small amounts of Sr^{2+}, and particularly on the selectivity of the materials for Sr^{2+} at a low concentration in a very saline media. Thus, Fig. 10b represents the evolution of the distribution coefficients K_d of the LTA zeolite, and the MG and MGZ27 materials as a function of the equilibrium Sr^{2+} concentration, after performing measurements in saline solutions with different Sr^{2+} concentrations.

At very low Sr^{2+} concentrations, where the selectivity of the materials for Sr^{2+} is estimated, the K_d values of the different materials can be determined. Note that these K_d values are higher than those determined previously using the preliminary experiments (Fig. 8) because the complete isotherms analyze the materials performance at lower $[Sr^{2+}]$. Although the MG material presents a slight selectivity for Sr^{2+}, the adsorption behavior of the composite is mainly controlled by the zeolite phase. Indeed, the K_d value measured for the MGZ27 material, ~2150 mL g^{-1}, is intermediate between the values measured for the pure LTA zeolite particles (~5530 mL g^{-1}) and the geopolymer MG (~1160 mL g^{-1}).

Note that the theoretical calculated K_d value based on the composition of the MGZ27 material (Eq. (4)) is ~2340 mL g^{-1}. This slight discrepancy between measured and calculated values of the distribution coefficient could be attributed to the presence of zeolite particles aggregates and/or the lower porosity of the geopolymer phase, which may decrease the accessibility of a small part of the zeolite particles.

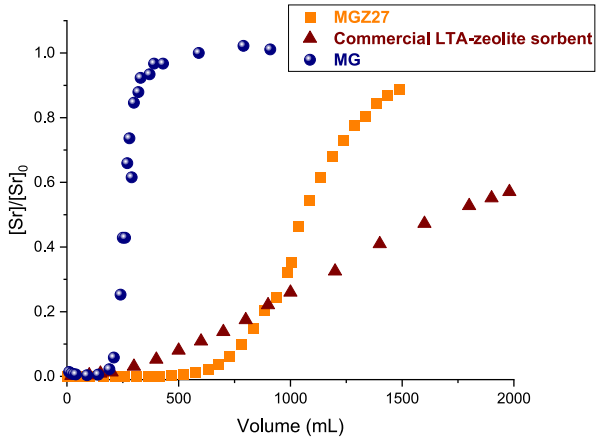

Fig. 11. Comparison of breakthrough curves measured for the macroporous geopolymer materials with 0 and 27 wt% of LTA zeolite particles (MG in blue circles and MGZ27 in orange squares) and for a commercial LTA zeolite adsorbent (brown triangles). (For interpretation of the references to colour in this figure legend, the reader is referred to the Web version of this article.)

Finally, these results highlight the benefits of the both phases of the composite material for Sr^{2+} sorption: the LTA zeolite particles increase both the material capacity and selectivity for Sr^{2+} in a saline solution, while the granular shaping of these particles in a hierarchically porous geopolymer allows the use of the material in a column process.

3.3. Sr^{2+} extraction in column process: comparison of the MG and MGZ27 with a commercial sorbent

Fig. 11 compares the breakthrough curves measured for the MG and MGZ27 materials, and for a commercial granular LTA zeolite sorbent.

These breakthrough curves illustrate the adsorption efficiency of the different materials regarding Sr^{2+} by plotting the outlet concentration $[Sr^{2+}]$ normalized by the inlet concentration $[Sr^{2+}]_0$ as a function of the amount of liquid waste that had passed through the column. At the beginning, the liquid waste feds the column and all the Sr^{2+} ions are adsorbed by the material, so the outlet concentration is zero. Then, when first Sr^{2+} ions are detected, the column is not completely efficient

Table 1
Parameters obtained by the Boltzmann modeling and input data of the breakthrough curves of the MG and MGZ27 materials.

Sample	$[Sr]_0$ mg L^{-1}	Mass g	Q_{batch} mg.g^{-1}	dV mL	Q_{dyn} mg.g^{-1}	Vb mL	Vr mL	Vm mL	V_r/V_m
MG	91.0	1.060	24.8	23.83	22.4	151.9	261.4	370.9	0.71
MGZ27	93.4	1.809	52.4	121.0	53.9	488.0	1044	1600.0	0.65

anymore while some parts of the column are still adsorbing Sr^{2+} ions. Finally, when the material in the whole column is saturated, the outlet concentration $[Sr^{2+}]$ is equivalent to the inlet concentration $[Sr^{2+}]_0$. Some specific points on the breakthrough curve can therefore be defined:

- The breakthrough volume V_b, at which $[Sr^{2+}]_{outlet} = 0.01[Sr^{2+}]_0$. This volume is directly linked with the first Sr^{2+} ions leak.
- The half-breakthrough volume V_r, at which $[Sr^{2+}]_{outlet} = 0.5[Sr^{2+}]_0$
- The breakthrough end volume V_m, at which $[Sr^{2+}]_{outlet} = 0.99\ [Sr^{2+}]_0$, before the outlet concentration reaches a plateau.

The shape of the curves depends on the interaction between the materials inside the column and the Sr^{2+} ions. The V_b value corresponds to the effluent volume after which the column has to be replaced. Indeed, from this point, Sr^{2+} ions are detected and the effluent is not perfectly decontaminated anymore. An early breakthrough, relative to a small V_b, indicates that the material adsorbed few contaminants. In the case of a nuclear decontamination operation, the breakthrough volume V_b is a critical point because, as soon as contamination passes through the column, the column is not viable anymore. The commercial adsorbent presents a very low V_b and its breakthrough curve is extremely flat. Consequently, even if the volume to completely saturate the column (V_m) is important, this material is not efficient to be used in a fixed-bed process. As this adsorbent is composed of LTA zeolite efficient to trap Sr^{2+}, this early breakthrough comes from a slow kinetic adsorption, which is confirmed by the flat breakthrough curve. As the sorption kinetic of the MG and MGZ27 materials are very fast due to their porous structure, their breakthrough curves are much straighter. Moreover, even if their volumes V_m are lower than the commercial sorbent, their V_b are higher, which is crucial for a nuclear decontamination operation. These materials are thus way more adapted to be used in a column process. To interpret and compare the overall efficiency of the MG and MGZ27 in a column process, the Boltzmann-sigmoid model can be used to fit the breakthrough curves, notably because the breakthrough fronts are symmetric. This model is described as followed [2,54]:

$$[Sr]_{outlet} = [Sr]_0 - \frac{[Sr]_0}{1 + \exp\left(\frac{V - V_r}{dV}\right)} \quad (6)$$

With dV the width of the sigmoid.

This leads to $V_b = V_r + dV * \ln\left(\frac{100}{99} - 1\right)$ and $V_m = V_r + dV * ln(99)$.

The fitting of the experimental breakthrough curves of the MG and MGZ27 materials are presented in Figure S5 and Table 1 reports the parameters obtained from these fitting. Table 1 also presents the input data of the both experiments ($[Sr^{2+}]_0$ value and the weight of adsorbent into the column) as well as the batch capacity of the materials, Q_{batch} at the Sr^{2+} concentration equilibrium of 90 mg L^{-1} obtained from the modeling of the isotherms (see Figure S3).

First, it is noteworthy that the batch sorption capacities (Q_{batch}) are tantamount to the total capacities of the column (Q_{dyn}, determined at the end of the experiment) for both samples, proving that all the material adsorption sites are accessible in the column. Then, the correlation coefficient (R^2) values are above 0.99 for the Boltzmann fitting of the two breakthrough curves, meaning that the model is reliable. The breakthrough occurs later for the MGZ27 material than for the MG one, as illustrated by the higher V_b extracted from the model. Indeed, the zeolite particles embedded in the MGZ27 increase the material capacity (Fig. 10a), and consequently the column capacity. Moreover, as the MGZ27 has a higher density than the MG, a larger mass is added in the column for an equal bed volume, which improves the whole column capacity.

Then, the Vr/Vm value can be related to the column efficiency. When this ratio is close to 1, the breakthrough curve is sharp and the global column efficiency is higher, regarding the material adsorption performances. The breakthrough curve of the MG material is straighter than the MGZ27 one, which is confirmed by the value of the column efficiency (V_r/V_m is higher for MG than for MGZ27, see Table 1). This could come from a direct impact of the material microstructure on the Sr^{2+} sorption performances. Indeed, the loading of 27 %wt of zeolite particles affects the geometry of the macroporous network and induces a drop of the geopolymer mesoporosity. This slows the sorption kinetic (Fig. 9), which may be responsible of a flatter breakthrough curve.

Finally, the column filled with the MGZ27 material presents the best performance in terms of wastewater decontamination (higher V_b and larger whole capacity) but the column filled with MG better optimizes the material sorption performances (higher V_r/V_m).

4. Conclusions

This article describes an emulsion-templating route for the synthesis of hierarchically porous composites consisting of a dispersion of LTA zeolite particles in a geopolymer binder. These materials possess a macroporous network that replicates the network of droplets in the initial emulsion on top of the geopolymer's intrinsically mesoporous nature. The composites described in this study are promising for the selective extraction of Sr^{2+} from highly saline media. They are notably particularly adapted of the decontamination of neutral and basic wastewater, due to the dissolution risk of the geopolymer in acidic media.

Comparisons between different formulations demonstrated that the material with the highest zeolite content is not necessarily the best choice for column processes, as the microstructural properties and mechanical robustness of the materials begin to degrade above a certain zeolite particle concentration. The optimal compromise between the macro- and microstructural properties of the material and the Sr^{2+} adsorption properties (capacity and selectivity) was identified. The selected material, containing 27 wt% zeolite particles, outperformed a commercial sorbent in a laboratory-scale column extraction experiment. Further investigations of the behaviour of this material in column processes would be beneficial. In particular, the impact of various processing parameters (column height, effluent velocity …) could be evaluated to determine the application range of the material. Moreover, a straight comparison of these materials with other adsorbents could be interesting. For that, the influence of the wastewater composition on the sorption properties should be performed to compare the different adsorbent performances in similar conditions.

Declaration of competing interest

The authors declare that they have no known competing financial interests or personal relationships that could have appeared to influence the work reported in this paper.

Acknowledgements

This work was supported by ORANO and the CEA energy division's

cross-cutting basic research programme (RTA Program). The authors thank David Lambertin and Nicolas Fabrègue for help developing the geopolymer formulation and Benoît Meilleray for performing some elementary analyses.

Appendix A. Supplementary data

Supplementary data to this article can be found online at https://doi.org/10.1016/j.ceramint.2024.03.090.

References

[1] F. Lorignon, A. Gossard, M. Carboni, Hierarchically porous monolithic MOFs: an ongoing challenge for industrial-scale effluent treatment, Chem. Eng. J. 393 (2020) 124765.
[2] A. Grandjean, Y. Barre, A. Hertz, V. Fremy, J. Mascarade, E. Louradour, T. Prevost, Comparing hexacyanoferrate loaded onto silica, silicotitanate and chabazite sorbents for Cs extraction with a continuous-flow fixed-bed setup: methods and pitfalls, Process Saf. Environ. Protect. 134 (2020) 371–380.
[3] B. Coasne, A. Galarneau, C. Gerardin, F. Fajula, F. Villemot, Molecular simulation of adsorption and transport in hierarchical porous materials, Langmuir 29 (2013) 7864–7875.
[4] A. Galarneau, A. Sachse, B. Said, C.H. Pelisson, P. Boscaro, N. Brun, L. Courtheoux, N. Olivi-Tran, B. Coasne, F. Fajula, Hierarchical porous silica monoliths: a novel class of microreactors for process intensification in catalysis and adsorption, Compt. Rendus Chem. 19 (2016) 231–247.
[5] S. Petlitckaia, Y. Barre, T. Piallat, O. Grauby, D. Ferry, A. Poulesquen, Functionalized geopolymer foams for cesium removal from liquid nuclear waste, J. Clean. Prod. 269 (2020) 122400.
[6] C. Delchet, A. Tokarev, X. Dumail, G. Toquer, Y. Barre, Y. Guari, C. Guerin, J. Larionova, A. Grandjean, Extraction of radioactive cesium using innovative functionalized porous materials, RSC Adv. 2 (2012) 5707–5716.
[7] C. Oster, M. Kaminski, J. Jerden, Y. Franchini, M. Magnuson, Evaluating solid sorbents for recycling wash waters containing strontium and calcium, J. Hazard. Toxic Radioact. Waste 23 (2019).
[8] S. Kwon, Y. Choi, B.K. Singh, K. Na, Selective and rapid capture of Sr2+ with LTA zeolites: effect of crystal sizes and mesoporosity, Appl. Surf. Sci. 506 (2020) 145029.
[9] A. Sachse, A. Merceille, Y. Barre, A. Grandjean, F. Fajula, A. Galarneau, Macroporous LTA-monoliths for in-flow removal of radioactive strontium from aqueous effluents: application to the case of Fukushima, Microporous Mesoporous Mater. 164 (2012) 251–258.
[10] K.M. Abd El-Rahman, A.M. El-Kamash, M.R. El-Sourougy, N.M. Abdel-Moniem, Thermodynamic modeling for the removal of Cs+, Sr2+, Ca2+ and Mg2+ ions from aqueous waste solutions using zeolite A, J. Radioanal. Nucl. Chem. 268 (2006) 221–230.
[11] W.F. Hao, N.N. Yan, M. Xie, X.J. Yan, X.L. Guo, P. Bai, P. Guo, T. Cheng, W.F. Yan, Origin of the exceptional selectivity of NaA zeolite for the radioactive isotope 90Sr2+, Inorg. Chem. Front. 9 (2022) 6258–6270.
[12] S. Shanmugam, Granulation techniques and technologies: recent progresses, Bioimpacts 5 (2015) 55–63.
[13] C. Algieri, E. Drioli, Zeolite membranes: synthesis and applications, Sep. Purif. Technol. 278 (2022) 119295.
[14] A.K. Vipin, S. Ling, B. Fugetsu, Removal of Cs+ and Sr2+ from water using MWCNT reinforced Zeolite-A beads, Microporous Mesoporous Mater. 224 (2016) 84–88.
[15] A.M. Escamilla-Pérez, Y. Barré, A. Grandjean, A. Hertz, Two-step synthesis of a macroporous LTA zeolite sorbent by supercritical CO2 coating and hydrothermal conversion: implementation in fixed-bed nuclear wastewater treatment, J. Supercrit. Fluids 199 (2023) 105940.
[16] A. Khalil, R. Hashaikeh, N. Hilal, 3D printed zeolite-Y for removing heavy metals from water, J. Water Process Eng. 42 (2021) 102187.
[17] F. Lorignon, A. Gossard, M. Carboni, D. Meyer, From wastes to interconnected porous monolith: upcycling of Al-based metal organic framework via pickering emulsion template, Mater. Lett. 296 (2021) 129931.
[18] Y.F. Zhu, W.B. Wang, H. Yu, A.Q. Wang, Preparation of porous adsorbent via Pickering emulsion template for water treatment: a review, J. Environ. Sci. 88 (2020) 217–236.
[19] Y. Sun, Y. Zhu, S.M. Zhang, B.P. Binks, Fabrication of hierarchical macroporous ZIF-8 monoliths using high internal phase pickering emulsion templates, Langmuir 37 (2021) 8435–8444.
[20] F. Lorignon, A. Gossard, S. Medjouel, M. Carboni, D. Meyer, Controlling polyHIPE surface properties by tuning the hydrophobicity of MOF particles stabilizing a pickering emulsion, ACS Appl. Mater. Interfaces 15 (2023) 30707–30716.
[21] A. Gossard, N. Fabregue, A. Hertz, A. Grandjean, High internal phase emulsions stabilized by a zeolite-surfactant combination in a composition-dependent manner, Langmuir 35 (2019) 17114–17121.
[22] Z.G. Cui, L.L. Yang, Y.Z. Cui, B.P. Binks, Effects of surfactant structure on the phase inversion of emulsions stabilized by mixtures of silica nanoparticles and cationic surfactant, Langmuir 26 (2010) 4717–4724.
[23] T. Nallamilli, M.G. Basavaraj, Synergistic stabilization of Pickering emulsions by in situ modification of kaolinite with non ionic surfactant, Appl. Clay Sci. 148 (2017) 68–76.
[24] A. Gossard, N. Fabregue, T. David, A. Grandjean, Effects of the zeolite concentration on the microstructure of high internal phase emulsions stabilized by surfactant-coated zeolite particles, Colloids Surf. A Physicochem. Eng. Asp. 625 (2021) 126853.
[25] M. Sandanayake, C. Gunasekara, D. Law, G.M. Zhang, S. Setunge, Greenhouse gas emissions of different fly ash based geopolymer concretes in building construction, J. Clean. Prod. 204 (2018) 399–408.
[26] V. Cantarel, F. Nouaille, A. Rooses, D. Lambertin, A. Poulesquen, F. Frizon, Solidification/stabilisation of liquid oil waste in metakaolin-based geopolymer, J. Nucl. Mater. 464 (2015) 16–19.
[27] C. Chlique, D. Lambertin, P. Antonucci, F. Frizon, P. Deniard, XRD analysis of the role of cesium in sodium-based geopolymer, J. Am. Ceram. Soc. 98 (2015) 1308–1313.
[28] T. Luukkonen, A. Heponiemi, H. Runtti, J. Pesonen, J. Yliniemi, U. Lassi, Application of alkali-activated materials for water and wastewater treatment: a review, Rev. Environ. Sci. Biotechnol. 18 (2019) 271–297.
[29] F. Elmahdoubi, S. Mabroum, R. Hakkou, M. Ibnoussina, Geopolymer materials based on natural pozzolans from the Moroccan middle atlas, Minerals 11 (2021) 1344.
[30] L.P. Qian, L.Y. Xu, Y. Alrefaei, T. Wang, T. Ishida, J.G. Dai, Artificial alkali-activated aggregates developed from wastes and by-products: a state-of-the-art review, Resour. Conserv. Recycl. 177 (2022) 105971.
[31] Z.H. Xu, Z. Jiang, D.D. Wu, X. Peng, Y.H. Xu, N. Li, Y.J. Qi, P. Li, Immobilization of strontium-loaded zeolite A by metakaolin based-geopolymer, Ceram. Int. 43 (2017) 4434–4439.
[32] I. Luhar, S. Luhar, M.M.A. Abdullah, R.A. Razak, P. Vizureanu, A.V. Sandu, P. D. Matasaru, A state-of-the-art review on innovative geopolymer composites designed for water and wastewater treatment, Materials 14 (2021) 7456.
[33] C. Reeb, C. Pierlot, C. Davy, D. Lambertin, Incorporation of organic liquids into geopolymer materials - a review of processing, properties and applications, Ceram. Int. 47 (2021) 7369–7385.
[34] A. Barneoud-Chapelier, J. Causse, A. Poulesquen, Synthesis of geopolymer emulsions, Mater. Lett. 276 (2020) 128188.
[35] D. Medpelli, J.M. Seo, D.K. Seo, Geopolymer with hierarchically meso-/macroporous structures from reactive emulsion templating, J. Am. Ceram. Soc. 97 (2014) 70–73.
[36] A. Gossard, G. Toquer, J. Causse, A. Grandjean, Monolithic zirconia foams synthesis from emulsion stabilized by colloidal clusters, Chem. Eng. J. 285 (2016) 528–535.
[37] C. Dong, J. Huang, Z.Y. Li, Y.Z. Chen, W. Wei, Z.J. Liu, Fabrication of conductive thermoplastic composites by supercritical fluid extraction of Pickering emulsion method, J. Supercrit. Fluids 180 (2022) 105445.
[38] V. Benavent, F. Frizon, A. Poulesquen, Effect of composition and aging on the porous structure of metakaolin-based geopolymers, J. Appl. Crystallogr. 49 (2016) 2116–2128.
[39] C. Michel, Y. Barre, M. Ben Guiza, C. de Dieuleveult, L. De Windt, A. Grandjean, Breakthrough studies of the adsorption of Cs from freshwater using a mesoporous silica material containing ferrocyanide, Chem. Eng. J. 339 (2018) 288–295.
[40] V. Proust, A. Gossard, J. Schaeperkoetter, S. Vannier, T. David, Y. Barre, S. Misture, A. Grandjean, H.C. zur Loye, Design and characterization of hierarchical aluminosilicate composite materials for Cs entrapment: adsorption efficiency tied to microstructure, J. Water Process Eng. 51 (2023) 103381.
[41] A. Gossard, A. Grandjean, D. Lambertin, N. Fabrègue, Solid Material Having an Open Multiple Porosity, Comprising a Geopolymer and Solid Particles, and Method for the Preparation Thereof, Patent, 2021. WO2021/152248.
[42] M.A. Longhi, B. Walkley, E.D. Rodríguez, A.P. Kirchheim, Z.H. Zhang, H. Wang, New selective dissolution process to quantify reaction extent and product stability in metakaolin-based geopolymers, Compos. B Eng. (2019) 176.
[43] C. Kuenzel, L. Li, L. Vandeperre, A.R. Boccaccini, C.R. Cheeseman, Influence of sand on the mechanical properties of metakaolin geopolymers, Construct. Build. Mater. 66 (2014) 442–446.
[44] V.F.F. Barbosa, K.J.D. MacKenzie, C. Thaumaturgo, Synthesis and characterisation of materials based on inorganic polymers of alumina and silica: sodium polysialate polymers, Int. J. Inorg. Mater. 2 (2000) 309–317.
[45] K.S.W. Sing, D.H. Everett, R.A.W. Haul, L. Moscou, R.A. Pierotti, J. Rouquerol, T. Siemieniewska, Reporting physisorption data for gas solid systems with special reference to the determination of surface-area and porosity (recommandations 1984), Pure Appl. Chem. 57 (1985) 603–619.
[46] M. Manko, J. Vittenet, J. Rodriguez, D. Cot, J. Mendret, S. Brosillon, W. Makowski, A. Galarneau, Synthesis of binderless zeolite aggregates (SOD, LTA, FAU) beads of 10, 70 mu m and 1 mm by direct pseudomorphic transformation, Microporous Mesoporous Mater. 176 (2013) 145–154.
[47] J. Rouyer, V. Benavent, F. Frizon, A. Poulesquen, Influence of geopolymer formulation parameters on the elastic and porous properties over a one-year monitoring, Mater. Lett. 207 (2017) 121–124.
[48] T.H. Tan, K.H. Mo, T.C. Ling, S.H. Lai, Current development of geopolymer as alternative adsorbent for heavy metal removal, Environ. Technol. Innov. 18 (2020) 100684.
[49] A.A. Siyal, M.R. Shamsuddin, M.I. Khan, N.E. Rabat, M. Zulfiqar, Z. Man, J. Siame, K.A. Azizli, A review on geopolymers as emerging materials for the adsorption of heavy metals and dyes, J. Environ. Manag. 224 (2018) 327–339.

[50] A. Merceille, E. Weinzaepfel, Y. Barre, A. Grandjean, The sorption behaviour of synthetic sodium nonatitanate and zeolite A for removing radioactive strontium from aqueous wastes, Sep. Purif. Technol. 96 (2012) 81–88.
[51] S. Chitra, S. Viswanathan, S.V.S. Rao, P.K. Sinha, Uptake of cesium and strontium by crystalline silicotitanates from radioactive wastes, J. Radioanal. Nucl. Chem. 287 (2011) 955–960.
[52] A. Villard, B. Siboulet, G. Toquer, A. Merceille, A. Grandjean, J.F. Dufreche, Strontium selectivity in sodium nonatitanate Na(4)Ti(9)O(20.)xH(2)O, J. Hazard Mater. 283 (2015) 432–438.
[53] X.B. Niu, Y. Elakneswaran, C.R. Islam, J.L. Provis, T. Sato, Adsorption behaviour of simulant radionuclide cations and anions in metakaolin-based geopolymer, J. Hazard Mater. 429 (2022) 128373.
[54] S.C. Motshekga, S.S. Ray, Highly efficient inactivation of bacteria found in drinking water using chitosan-bentonite composites: modelling and breakthrough curve analysis, Water Res. 111 (2017) 213–223.